Bottom-Up Fabrication of Plasmonic Nanoantenna-Based High-throughput Multiplexing Biosensors for Ultrasensitive Detection of microRNAs Directly from Cancer Patients' Plasma

Adrianna N. Masterson[1], Thakshila Liyanage[1], Hristos Kaimakliotis[2], Hamed Gholami Derami[3],

Frédérique Deiss[1], Rajesh Sardar[1,4*]

[1]Department of Chemistry and Chemical Biology, Indiana University-Purdue University Indianapolis, 402 N Blackford Street, Indianapolis, Indiana 46202, United States

[2]Department of Urology, Indiana University School of Medicine, 535 N. Barnhill Dr. Indianapolis, Indiana 46202, United States

[3]Department of Mechanical Engineering and Materials Science, Institute of Materials Science and Engineering, Washington University in St. Louis, Saint Louis, Missouri 63130, United States

[4]Integrated Nanosystems Development Institute, Indiana University-Purdue University Indianapolis, 723 W. Michigan Street, Indianapolis, Indiana 46202, United States

*Corresponding author email: rsardar@iupui.edu

ABSTRACT

There is an unmet need in clinical point-of-care (POC) cancer diagnostics for early state disease detection, which would greatly increase patient survival rates. Currently available analytical techniques for early stage cancer diagnosis do not meet the requirements for POC of a clinical setting. They are unable to provide the high demand of multiplexing, high-throughput, and ultrasensitive detection of biomarkers directly from low volume patient samples ("liquid biopsy"). To overcome these current technological bottle-necks, herein we present, for the first time, a bottom-up fabrication strategy to develop plasmonic nanoantenna-based sensors that utilize the unique localized surface plasmon resonance (LSPR) properties of chemically synthesized gold nanostructures, gold triangular nanoprisms (Au TNPs), gold nanorods (Au NRs), and gold spherical nanoparticles (Au SNPs). Our Au TNPs, NRs, and SNPs display refractive index unit (RIU) sensitivities of 318, 225, and 135 nm/RIU respectively. Based on the RIU results, we developed plasmonic nanoantenna-based multiplexing and high-throughput biosensors for the ultrasensitive assay of microRNAs. MicroRNAs are directly linked with cancer development, progression, and metastasis, thus they hold promise as next generation biomarkers for cancer diagnosis and prognosis. The developed biosensors are capable of assaying five different types of microRNAs at an attomolar detection limit. These sets of microRNAs include both oncogenic and tumor suppressor microRNAs. To demonstrate the efficiency as a POC cancer diagnostic tool, we analyzed the plasma of 20-bladder cancer patients without any sample processing steps. Importantly, our liquid biopsy-based biosensing approach is capable of differentiating healthy from early ("non-metastatic") and late ("metastatic") stage cancer with a p value < 0.0001. Further, receiver operating characteristic analysis shows that our biosensing approach is highly specific, with an area under the curve of 1.0. Additionally, our plasmonic nanoantenna-based biosensors are regenerative, allowing multiple measurements using the same sensors, which is essential in low- and middle-income countries. Taken together, our multiplexing and high-throughput biosensors have the unmatched potential to advance POC diagnostics and meet global needs for early stage detection of cancer and other diseases (e.g., infectious, autoimmune and neurogenerative diseases).

INTRODUCTION

In this article, we report for the first time a bottom-up fabrication approach for nanoplasmonic sensors containing chemically synthesized plasmonic nanostructures ("*nanoantennas*") (e.g., gold triangular nanoprisms (Au TNPs), gold nanorods (Au NRs), or gold spherical nanoparticles (Au SNPs)). The unique and highly sensitive localized surface plasmon resonance (LSPR) properties of these nanostructures,[1-4] along with the generality of the fabrication method utilized, obviate the undesirable optical and structural effects associated with lithographically prepared nanostructures for sensing applications. Key advantages of this new approach include: (1) enhanced sensing efficiency, (2) prevention of aerobic oxidation, (3) avoidance of fast structural changes in real biological fluids, (4) preclusion of expensive and labor extensive sensor fabrication steps, and (5) demonstrated assay capabilities for real-world clinical samples.[2, 5] These advantages are critical for the design of a multiplexing, high-throughput assay suitable for point-of-care (POC) diagnostics and that satisfies global needs. Utilizing our plasmonic nanoantenna-based biosensors, we now are capable of successfully assaying five different types of microRNAs ("multiplexing") from multiple patient samples ("high-throughput") simultaneously using one absorbance instrumentation with a simple plate reader in one instrument run.

Multiplexed biological assays are important for POC diagnostic purposes as they offer several key advantages such as low sample volume, short assay time, and simultaneous detection of multiple biomarkers in one instrumentation run. Current multiplexing bioanalytical assays for disease-related biomarkers (e.g., nucleic acids and proteins) include genotyping,[6, 7] enzyme-linked immunosorbent assay (ELISA),[8-10] fluorescence,[11, 12] hydrogel microparticles,[13] and electrochemical techniques,[14-16] all which have many challenges including low sensitivity, low specificity, and the need for extensive sample purification steps that together hinder the ability to achieve ultra-high sensitivity (e.g., fg/μL) for early-stage cancer diagnosis. Furthermore, many of these current multiplexing assays also require a label to quantify the biomarker, therefore producing false responses due to unwanted interactions between labeled molecules and analytes of interest.

Aside from multiplexing, creating high-throughput assays is important in diagnostics, as this allows multiple tests to be conducted at once. This reduces delays in obtaining test results and improving the rapid identification and early detection of disease allows effective and timely treatment. In this context, over the last 30 years, biosensing approaches utilizing the unique LSPR properties of plasmonic nanoantennas have gained significant attention due to label-free and highly sensitive detection properties.[2, 17-19] Furthermore, LSPR-based biosensors demonstrated the ability to quantitative detection of disease-related biomarkers using low volume clinical samples without purification steps.[20-23] However, few LSPR-based multiplexing high-throughput assays have been reported for real world sample analysis. In particular, the use of LSPR-based assays in liquid biopsies has yet to be demonstrated.[12, 24, 25] Herein, we show a novel and highly scalable fabrication approach to create plasmonic nanoantenna-based biosensors that utilize a simple detection scheme, where signal readout is measured using a less expensive plate reader in the absorption mode, thus simplifying and lowering the cost of LSPR-based multiplexed, high-throughput biosensing.

We selected microRNAs to demonstrate the multiplexing and high-throughput assay capabilities of our newly designed plasmonic nanoantenna-based biosensors because not only are these small noncoding RNAs capable of regulating half of the human genes, but also a single microRNA can target several hundred of genes.[26-28] Furthermore, microRNAs are directly linked with cancer development, progression, and metastasis, and thus serve as next generation cancer biomarkers for diagnosis and prognosis.[28, 29] However, current state-of-the-art microRNA assays such as northern blotting, quantitative reverse transcription polymerase chain reactions (qRT-PCR), genotyping, and microarrays not only suffer from low specificity and low sensitivity, but also require the labelling and pre-amplification of microRNAs as well as multiple conversion steps for complementary DNAs. These methods are therefore impractical with real-life clinical samples that also demand exhausting, labor intensive and time-consuming sample preparation/purification steps. Additionally, during the multiple purification steps, loss of biomarkers is inevitable, thus the actual concentration of microRNA is difficult to determine; this could turn out to be detrimental in early stage for POC diagnosis of cancers. To overcome the current technological challenges in microRNA assays, we quantitatively analyzed two oncogenic (microRNA-10b and microRNA-96) and three tumor suppressor (microRNA-145, microRNA-

143, and microRNA-490-5p) microRNAs that are known to be bladder cancer (BC) specific.[23, 30-35] Using our plasmonic nanoantenna-based biosensors, these microRNAs are analyzed simultaneously with attomolar (aM) sensitivity.

As a proof-of-concept for the high-throughput capability of the plasmonic nanoantenna-based biosensors described herein, we assayed the above-mentioned microRNA sets in the plasma of 10 normal controls (NC, healthy individuals), 10 metastatic BC (MTBC) patients, and 10 non-metastatic BC (NMTBC) patients. One-way ANOVA analysis reveals that tumor suppressor microRNAs (microRNA-145, -143, and -490-5p) are more specific BC biomarkers than oncogenic microRNAs in separating the three patient groups from each other; resulting in p-values < 0.0001 for NC vs MTBC, NC vs. NMTBC, and MTBC vs. NMTBC patients. Furthermore, all five microRNAs displayed an area under the curve (AUC) of 1.0 from the receiver operating characteristics (ROC) analysis. The data suggest that this multiplexing microRNA assay has excellent separability between the control group (NC) and the disease group (MTBC or NMTBC patients).

EXPERIMENTAL SECTION

Materials. Chloro(triethylphosphine) gold (I) (Et$_3$PAuCl, 97%) and HAuCl$_4$ was purchased from Gelest Inc. Poly(methylhydrosiloxane) (PMHS, Mn = 1700-3300), triethylamine (TEA, 98%), sodium citrate (99.5%), hexadecyltrimethylammonium bromide (CTAB, 99%), D-(+)-Glucose (99.5%), sodium borohydride, silver nitrate (99%), L(+)-Ascorbic acid (reagent grade), ACS grade acetonitrile (CH$_3$CN, 99.9%), and methanol (99.8%) were purchased from Sigma-Aldrich. (3-Mercaptopropyl)-trimethoxysilane (MPTMS, 94%) was purchased from Alfa Aesar. Ethanol (200 proof) was purchased from Decon labs. Thiolated polyethylene glycols were purchased from purePEG. Thiol modified 3'-SH-(CH$_2$)$_3$-ssDNAs, microRNAs, and RNase H enzyme were purchased from Integrated DNA Technologies. All chemicals were used without further purifications. RNase free sterile water was obtained from Baxter Healthcare Corporation. 18x18 mm glass coverslips were purchased from Fisher Scientific. RBS 35 Detergent was obtained from Thermo Scientific and used as received. No-bottom 96-multiwell plates were purchased from Greiner Bio-One. Krazy Glue was purchased from Office Depot. All water was purified using a Thermo Scientific Barnstead Nanopure system. Thiol modified -ssDNAs, microRNAs, and patient samples were stored at -80 °C. PBS buffer (pH = 7.2) was prepared using RNase free sterile water. Ethanol was purged with N$_2$ for 30 min prior to use.

Spectroscopy and Microscopy Characterizations. Absorption and extinction spectra in the range of 400-1000 nm were collected with a SpectraMax M5 microplate reader from Molecular Devices, LLC. Extinction spectra of Au TNP, Au SNP, and Au NRs attached onto glass substrates were measured in air in order to determine the LSPR peak position (λ_{LSPR}). In the RIU sensitivity studies, extinction spectra of all nanostructures were recorded in aqueous glucose solutions. In the LSPR-based microRNA assays utilizing Au TNPs, all extinction spectra were recorded in PBS buffer. All extinction spectra were collected at room temperature. A silanized blank glass coverslip immersed in PBS buffer/aqueous glucose solution /air was used as a background and a plasmonic nanoantenna-based bionsensor incubated in PBS buffer/water/air was considered the reference (blank). The chemically synthesized Au TNPs, NRs, and SNPs attached onto the silanized glass coverslips inside the multiwell plates were characterized using scanning electron microscopy (SEM).

Bottom-Up Fabrication of Plasmonic Nanoantenna-Based Sensors and Refractive Index Unit Sensitivity Measurements. The fabrication strategy we developed involves: (1) Incubation of MPTMS-functionalized glass coverslips into a colloidal solution of freshly-synthesized plasmonic nanostructures (Au TNPs, NRs, or SNPs) overnight at room temperature; (2) Plasmonic nanostructure-bound glass coverslips were then thoroughly rinsed with nanopure water and dried under N_2 flow; (3) Resulting glass coverslips were then glued to a no-bottom 96-multiwell plate by applying a small amount of glue around the edges of the coverslip and gently placing it onto the bottom of the well plate; attached coverslips were allowed to dry for at least 4h at room temperature prior to further analysis. We also examined the proper fabrication of each well by incubating wells in nanopure water to confirm there was no water leakage. In the case of Au TNP-based sensors, we performed a tape-cleaning procedure to remove non-prismatic nanostructures, as described previously.[20-23] Briefly, tape cleaning was performed by placing adhesive scotch tape (3M corporation) onto the Au TNP-attached coverslips, gently pressed down with a finger, and then slowly removing the tape at a 90° angle. The refractive index unit (RIU) sensitivities for plasmonic nanoantenna-based sensors of differently-shaped nanostructures were measured as follows: After the bottom-up fabricated sensors of each plasmonic nanostructure were attached to the functionalized glass substrates, each well was incubated in 300 μL of water for 15 min. After that, LSPR extinction spectra were recorded. This process was repeated for different concentrations of aqueous glucose solutions (volume% = 0%, 10%, 15%, 20%, 30%, and 50%). Once all LSPR extinction spectra were collected, the wavelength maximum was recorded for each solution and graphed verses the refractive index of the solution. Linear regression was then performed using Excel and the RIU sensitivity (slope of regression equation) was obtained.

Design of Plasmonic Nanoantenna-Based Multiplexing and High-throughput microRNA Biosensors. After the bottom-up fabrication of Au TNPs plasmonic nanoantenna sensors, each well was incubated in 0.3 mL of a 1000:1 μM PBS buffer solution of 3'-SH-$(CH_2)_3$-ssDNA-X: PEG_4-SH mixture overnight, here X = -10b, -96, -143, -145, and -490-5p (see Table S1). Each

well was rinsed with a copious amount of PBS buffer to remove loosely bound materials before used for microRNA analyses. The plasmonic nanoantenna-based biosensors were stored in N_2 purged PBS buffer up to one week at 4 °C.

Development of microRNA Calibration Plots in Buffer and Human Plasma. The LSPR extinction spectra of plasmonic nanoantenna-based biosensors were collected in PBS buffer to determine λ_{LSPR}. Then, biosensors were incubated in a 0.3 mL microRNA solution of different concentrations (ranging from 10 nM to 100 aM) in PBS buffer (or 10 μL human plasma in 0.29 mL PBS buffer) overnight. MicroRNA-bound biosensors were washed with PBS buffer to remove any nonspecifically adsorbed biomolecules, and LSPR extinction spectra were collected and λ_{LSPR} was determined. False positive analysis was conducted by incubating the plasmonic nanoantenna-based microRNA biosensors in a human plasma without any microRNAs. False negative analysis was conducted by incubating only PEG_4-SH-functionalized plasmonic nanoantennas in 10 nM to 100 aM microRNA solutions. In the blank sample analysis, Au TNP-attached coverslips in the high-throughput configuration were incubated in different concentrations of microRNAs in human plasma and extinction spectra were collected.

Quantification of microRNA in Bladder Cancer Patient Samples. Plasmonic nanoantenna-based biosensors were incubated in a solution containing 10 μL of bladder cancer patient plasma (MT, NMT, and Normal control samples) diluted with 0.29 mL PBS buffer for overnight. The biosensors were then thoroughly washed with PBS buffer to remove any nonspecifically adsorbed biomolecules. LSPR extinction spectra were recorded, and λ_{LSPR} was determined for each patient/microRNA.

Data Processing and Statistical Analysis. The λ_{LSPR} was obtained by using the maxima of the UV-visible extinction spectra (determined through curve fitting using Origin software) and $\Delta\lambda_{LSPR}$ was derived by taking the difference between the λ_{LSPR} of the plasmonic nanoantenna-based biosensors before and after hybridization with the target microRNA. Calibration curves were obtained by plotting $\Delta\lambda_{LSPR}$ vs. microRNA concentration, with concentration being plotted on the axis in a logarithmic scale in order to investigate non-specific adsorption at a lower concentration range. The calibration curve equation was determined through linear regression using Excel. Finally, the LOD was determined by using the Z value of the blank ($Z = mean + 3\sigma$, σ = standard deviation), which was obtained from six $\Delta\lambda_{LSPR}$ measurements using the six different biosensors. Plugging the Z value into the "Y" in the calibration curve equation yielded the LOD concentration ("X"). Concentration of target microRNAs in patient samples were determined from the calibration curves developed in human plasma, with $\Delta\lambda_{LSPR}$ values and corresponding concentrations obtained from the average of six measurements. Each sample was independently analyzed twice (two weeks apart). Standard one-way ANOVA and area under the curve (AUC) of the receiver operating characteristic (ROC) graphs were plotted using GraphPad Prism. One-way ANOVA used the

following p value style: 0.1234 (ns), 0.0332 (*), 0.0021 (**), 0.0002 (***), <0.0001 (****), and was performed at the 95% confidence interval. AUC of ROC were also performed at the 95% confidence interval.
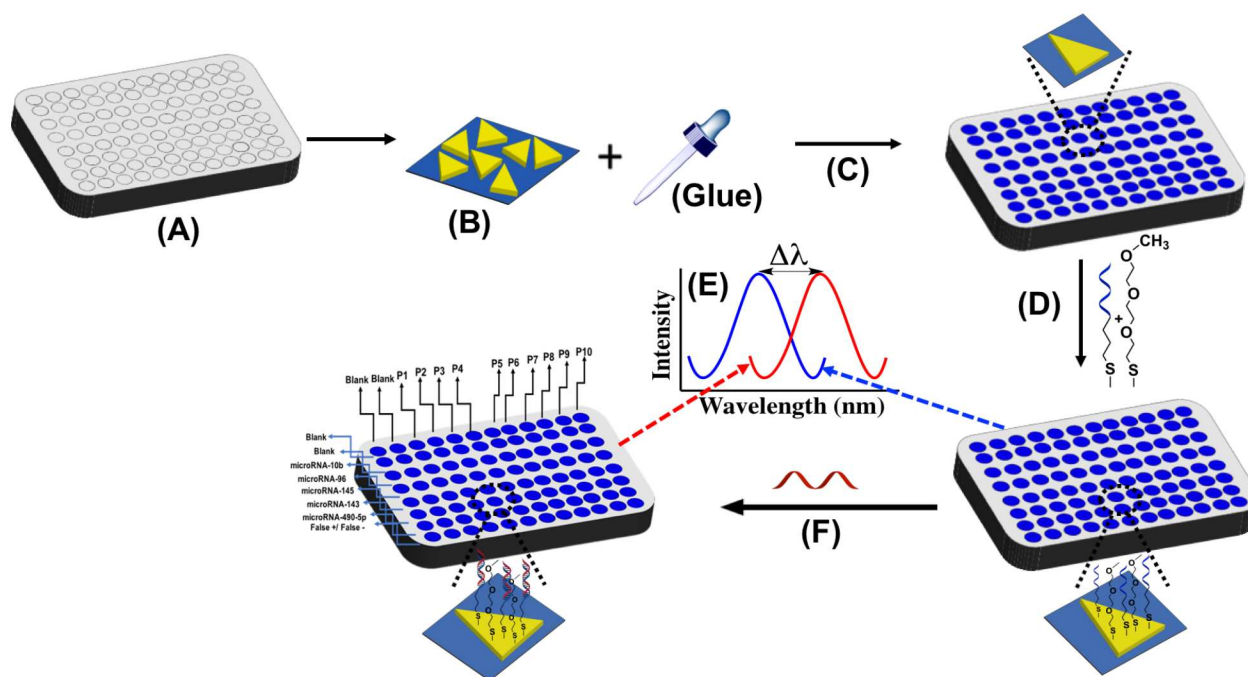
Scheme 1. Fabrication of plasmonic nanoantenna-based multiplexing and high-throughput biosensors for assaying numerous microRNAs using a 96 well plate. *(A) A no-bottom 96 well plate. (B) Chemically-synthesized Au TNPs are covalently attached onto a MPTMS functionalized glass coverslip. (C) Glass coverslips containing Au TNPs are then attached to the bottom of a 96 well plate. (D) The well plate is incubated in a solution of 3'-SH-(CH$_2$)$_3$-ssDNA-X and PEG$_4$-SH to develop biosensors. (E)The LSPR peak of plasmonic nanoantenna-based biosensor will be measured in PBS buffer (blue curve). The LSPR peak will be measured again after incubating the biosenosrs in microRNA solution (red curve).   (F) The as fabricated biosensors are then used to assay numerous microRNAs (multiplexing) as well as different patients simultaneouly (high-throughput).*

RESULTS AND DISCUSSION
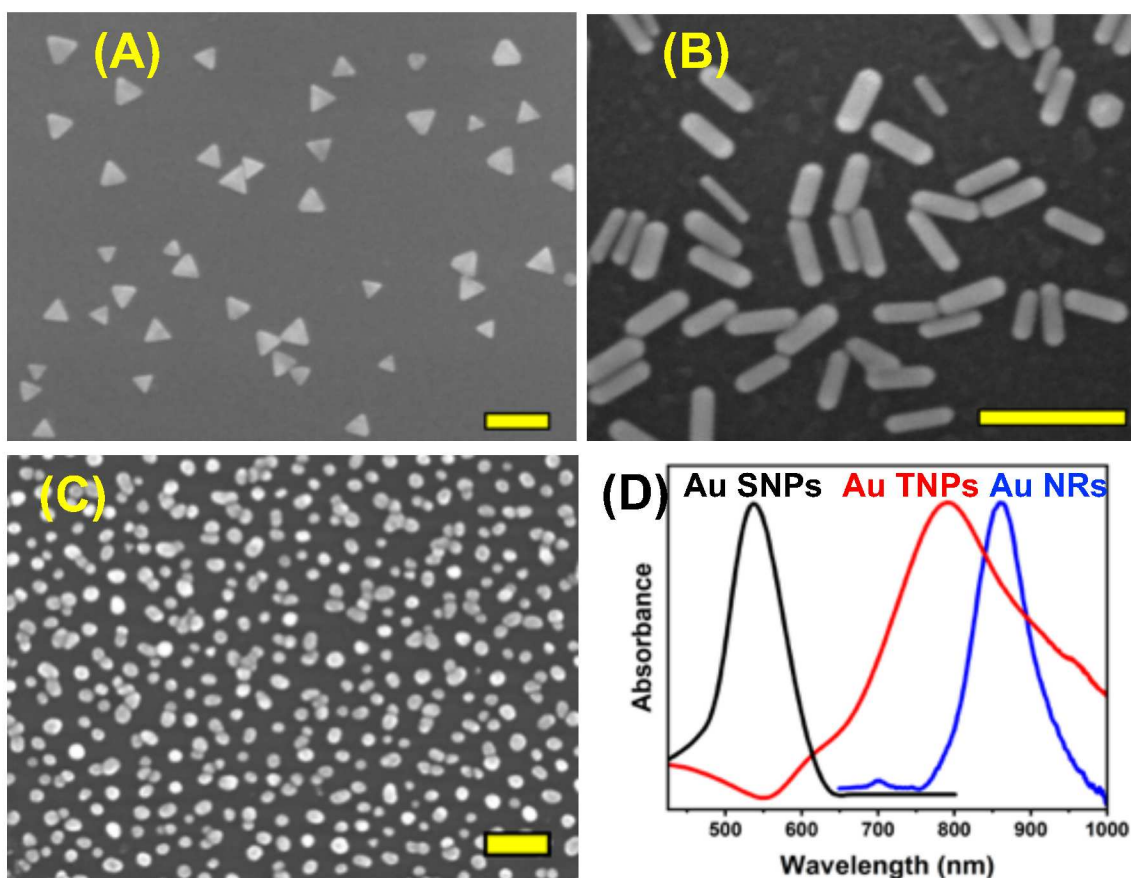
Figure 1. *A representative scanning electron microscopy image of Au TNPs (A), Au NRs (B), and Au SNPs (C). The scale bars are 100 nm. The dimension of the plasmonic nanostructures were determined using Image J software. (D) UV-visible extinction spectra of Au SNPs (black, λ_{LSPR} = 530 nm), Au NRs (blue, λ_{LSPR} = 860 nm), and Au TNPs (red, λ_{LSPR} = 795 nm) attached onto glass coverslips. All extinction spectra were collected in air.*

Plasmonic Nanostructure-Based Sensors Respond to the Bulk Refractive Index Change.

Scheme 1 illustrates the construction of our plasmonic nanoantenna-based multiplexing and high-throughput biosensors using chemically synthesized nanostructures. In order to generalize the bottom-up fabrication of sensors, we used three different shaped plasmonic nanostructures, Au SNPs, NRs, and TNPs that are commonly used in the development of efficient plasmonic nanoantenna-based biosensors.[1-3, 18] We chemically synthesized an average 42 nm edge length

and 8 nm thick Au TNPs, 47 nm long and 14 nm diameter Au NRs, and 38 nm diameter Au

SNPs. Supporting Information file provides detailed experimental procedure for the synthesis of

these nanostructures. **Figure 1A-C** shows scanning electron microscopy (SEM) images of the

three differently shaped nanostructures attached onto a glass substrate. Au TNPs, NRs, and Au

SNPs display LSPR extinction peaks (λ_{LSPR}) at 795, 860, and 530 nm, respectively, in air

(**Figure 1D**). Before examining their multiplexing biosensing abilities, we first examined the

refractive index sensitivity of Au TNPs, NRs, and SNPs in aqueous glucose solutions of varying

concentrations because it is important to determine that the nanostructures are optically

responsive to the refractive changes around them. As illustrated in **Figure 2A-C**, the λ_{LSPR}

gradually red-shifts with increasing glucose concentrations (an increase in refractive index of the

surrounding medium). Data are in agreement with the LSPR properties of plasmonic

nanostructures, as described by Mie theory.[1] **Figure 2D** demonstrates a linear response for λ_{LSPR}

as a function of the surrounding media refractive index. The RIU sensitivity of Au TNPs, NRs,

and SNPs is 318, 225, and 135 nm/RIU respectively. The highest RIU sensitivity of Au TNPs is

also in agreement due to their large shape factor compared to either NRs or SNPs.[36] It is well

known that the electromagnetic (EM) field around a metallic nanostructure is enhanced at the

sharp tips, edges, and corners due to polarization effects.[37] Such effects are minimal for

nanostructures with curved surfaces such as NRs and SNPs.[38] Our experimentally determined

RIU sensitivities for these nanostructures are comparable to literature reports in which RIU

sensitivity was measured on a flat glass coverslip without the multi-well configuration.[39, 40]

Therefore, it was expected that multiplexing and high-throughput biosensors could be designed

using the nanostructures within multi-well plates without compromising sensing efficiency.
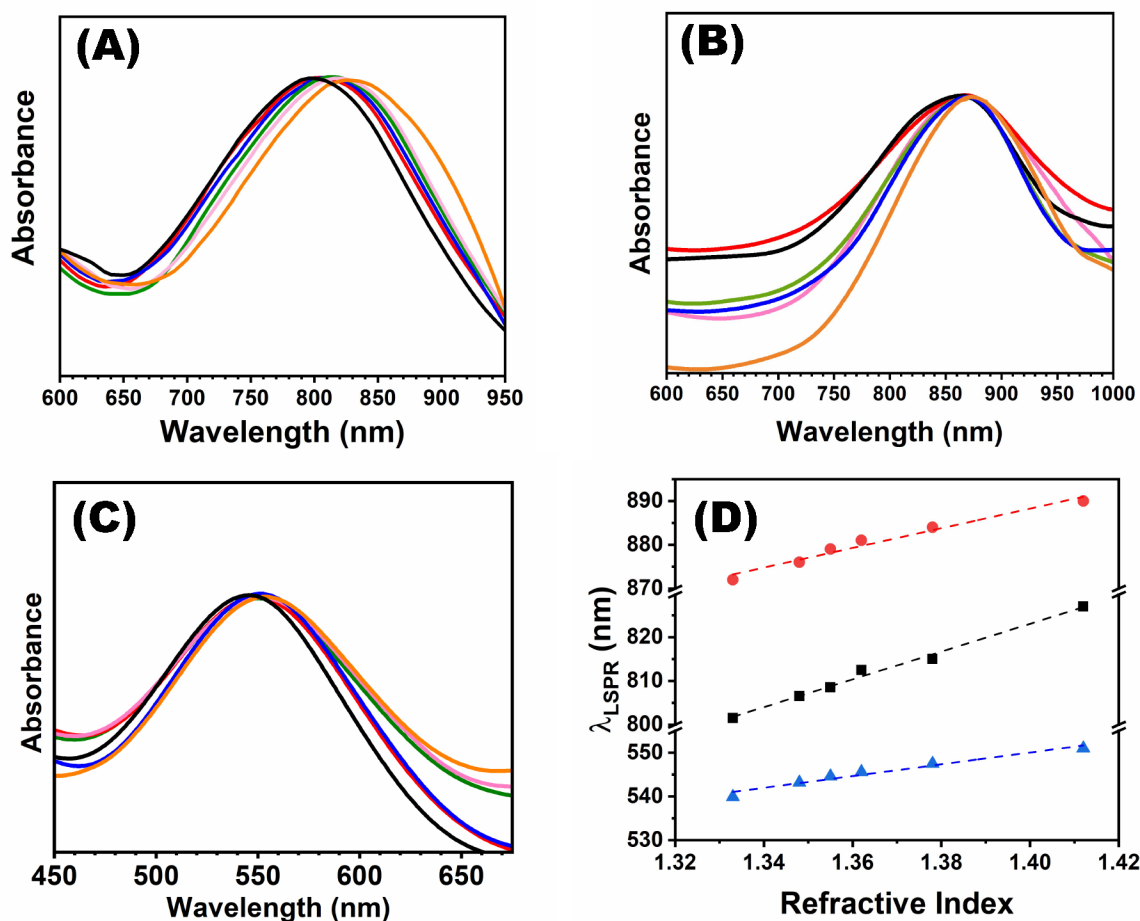
Figure 2. Refractive index sensitivity studies of plasmonic nanoantenna-based sensors. *UV-vis extinction spectra of gold nanostructures on silanized glass substrates; (A) Au TNPs, (B) Au NRs, and (C) Au SNPs in different concentration of aqueous glucose solutions. (Au TNPs: black-water-801.5 nm, red-10% glucose- 808 nm, blue-15% glucose-809.5 nm, green-20% glucose-813.5 nm, pink-30% glucose- 815 nm, orange-50% glucose- 824 nm/ Au nanorods: black-water-872 nm, red-10% glucose-876 nm, blue-15% glucose- 879 nm, green-20% glucose- 881 nm, pink-30% glucose- 884 nm, orange-50% glucose-890 nm / Au spherical particles: black-water- 539.9 nm, red-10% glucose- 543 nm, blue-15% glucose-544.6 nm, green-20% glucose- 545.6 nm, pink-30% glucose- 547.5 nm, orange-50% glucose- 551 nm). (D)Relationship between LSPR dipole peak position (λ_{LSPR} in nm) of the Au TNPs (black squares), Au NRs (red dots), or Au SNPs (blue triangles) and the refractive index of different concentrations of aqueous glucose solutions. The dashed lines are the linear trends, which display sensitivities of 318 nm/RIU (R^2 = 0.993), 225 nm/RIU (R^2 = 0.974), and 135 nm/RIU (R^2 = 0.961) respectively.*

MicroRNA Assay Through a Multiplexing and High-Throughput Approach. The highest RIU sensitivity prompted us to design microRNA biosensors using Au TNPs as plasmonic nanoantennas. **Figure S1A** depicts the LSPR response of Au TNPs during different functionalization steps and upon attachment of microRNAs. Functionalization of Au TNPs with SH-$(CH_2)_3$-ssDNA-10b: PEG_4-SH, which produces plasmonic nanoantenna-based microRNA biosensors, display an average ~35 nm red shift in λ_{LSPR}. This red shift is due to changes in TNP local refractive index. Upon addition of 10.0 nM of fully-complimentary microRNA-10, an additional 12 nm red-shift in λ_{LSPR} is observed. This unusually high LSPR response of our plasmonic nanoantenna-based microRNA biosensors towards microRNAs is due to wave function delocalizations of surface plasmon electrons rather than a simple refractive index change related mechanism.[23] We first performed an assay by developing a calibration curve of microRNA-10b and microRNA-145 in PBS buffer in order to demonstrate multiplexing abilities. As shown in **Figure S1B**, a linear trend over the range from 10 nM to 100 aM is observed with LODs of 98 aM for both microRNAs (**Table S3 and S4**). It is important to mention that we also attempted to design multiplexing microRNA biosensors using Au NRs under identical experimental conditions as described for TNPs. Surprisingly, we were unsuccessful at functionalizing Au NRs with a mixture of SH-$(CH_2)_3$-ssDNA-X: PEG_4-SH (data not shown). We believe that the CTAB bilayer on NRs did not allow an effective ligand exchange reaction for the direct attachment of SH-$(CH_2)_3$-ssDNA-X. Our observation is also supported by literature in which a ligand exchange of CTAB with a thiolated molecule, such as mercaptopropionic acid, was conducted before attachment of -ssDNA.[41-45] However, to the best of our knowledge, no report is available presenting attachment of SH-$(CH_2)_3$-ssDNA-X onto Au NRs via a direct ligand exchange reaction for biosensing applications. Nevertheless, our goal has been to develop a simplified biosensor for the microRNA assay without performing complicated ligand exchange chemistry to functionalize nanostructures.
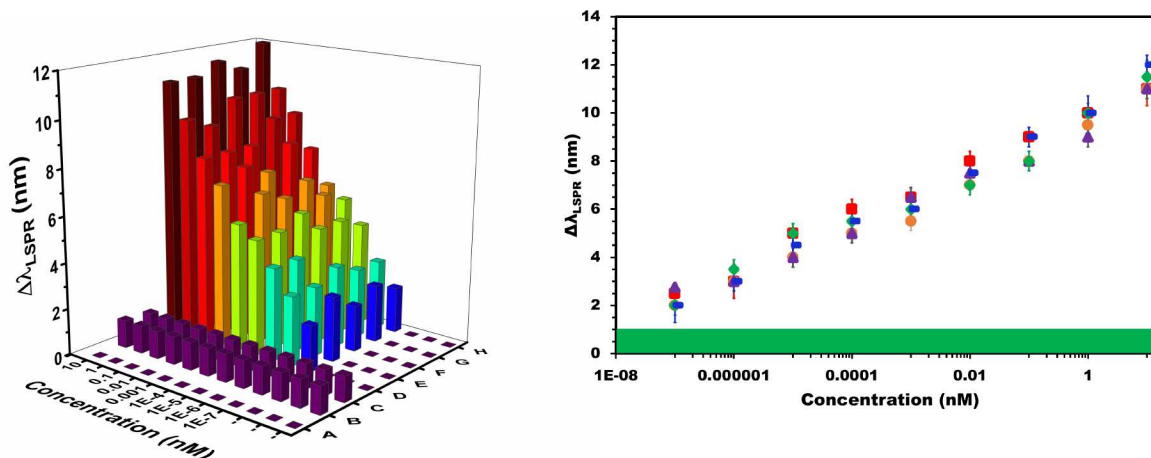
Figure 3. LSPR response of plasmonic nanoantenna-based biosensors for a different concentration of microRNAs in human plasma. (Left) *Average λ_{LSPR} shift ($\Delta\lambda_{LSPR}$) of biosensor as a function of microRNA concentration: A = blank, B= false positive, C = false negative, D = microRNA-145, E = microRNA-143, F = microRNA-490-5p, G = microRNA-10b, H = microRNA-96. In the false positive experiment, no microRNA was used. Purple bars represent $\Delta\lambda_{LSPR}$ values upon incubation of biosensors in human plasma without microRNAs. These values were used as the blank for LOD calculation.* ***(Right)*** *Calibration plot for* microRNA-*10b (red squares), microRNA-96 (blue rectangles), microRNA-145 (orange circles), microRNA-143 (purple triangles), and microRNA-490-5p (green diamonds). Each type of biosensor was constructed with corresponding –ssDNAs as receptor molecules. Calibration curves with the green bar represent three times the standard deviation of the blank (0.48 nm). Concentrations were plotted in logarithmic scale to determine non-specific adsorption of endogenous biomolecules from human plasma and/or microRNAs at a lower concentration range.*

The data presented above show that Au TNPs are the most suitable nanoantennas for microRNA detection and quantification. Therefore, TNPs were used to demonstrate feasibility for the multiplexing assay. We selected a total of five microRNAs (microRNA-10b, microRNA-96, microRNA-145, microRNA-143, and microRNA-490-5p) that are all reported to be highly specific biomarkers for early diagnosis of BC.[30, 32, 35] **Figure 3, Left** depicts the LSPR response ($\Delta\lambda_{LSPR}$) of biosensors for different microRNA concentrations in human plasma including blank, false positive and negative responses (see experimental section for details). The purpose of using human plasma as the media is to demonstrate the feasibility of our biosensors in clinical POC diagnostics, particularly liquid biopsies. We also developed calibration curves for all five microRNAs with a concentration range of 10.0 nM to 100.0 aM (**Figure 3, Right**). **Table S5 and S6** present all the raw values of $\Delta\lambda_{LSPR}$ at different concentrations of microRNAs. Our calculated LODs for microRNA-10b, microRNA-96, microRNA-145, microRNA-143, and microRNA-490-5p are 59, 89, 212, 186, and 183 aM, respectively. Furthermore, this is the first

example in which successful detection and ultrasensitive quantification of microRNAs has been demonstrated in a multiplexing set-up. **Figure 3, Left** also illustrates the experimentally determined LSPR response from 81 wells under one instrument run, demonstrating the high-throughput assay capability of our developed biosensors. It is important to mention that in the false positive/negative experiments, we observed an average $\Delta\lambda_{LSPR}$ of 0.8 nm with the highest value of 1.5 nm. We believe this measured $\Delta\lambda_{LSPR}$ value could be a combination of instrumental noise and/or non-specific adsorption of microRNAs onto glass substrates. In the latter case, we could still detect a very small $\Delta\lambda_{LSPR}$ value because Au TNPs display an extremely large sensing volume.[22] Nevertheless, we can confidently measure 100 aM concentrations of microRNA because it provides the lowest $\Delta\lambda_{LSPR}$ value of 2.0 nm, which is greater than the $\Delta\lambda_{LSPR}$ value obtained for false positive/false negative experiments.

The sensitivity of these plasmonic nanoantenna-based multiplexing microRNA biosensors is nearly 10^3-fold lower than our previously fabricated biosensors using a similar surface chemistry for a single LSPR measurement in a cuvette using a standard UV-visible spectrometer and a 3.0 mL analyte volume.[23] This could be due to the 10^3-fold difference in analyte solution volume used between two techniques. However, the advantage of using a low sample volume is that liquid biopsies can be conducted using small quantities of patient plasma, as described in a later part of this article. Furthermore, conducting single LSPR measurements at a time is labor extensive and time consuming, and these technological bottlenecks can be avoided by performing the assay through our newly developed multiplexed and high-throughput biosensors. Nevertheless, the LOD values we determined for five different microRNAs are much improved over other various multiplexed biosensors and are capable of quantifying microRNAs in both buffer and human biofluids, see **Table S7**.

We believe the exceptionally high sensitivity of our newly developed plasmonic nanoantenna-based multiplexing biosensors stems from the different and unique structural features of chemically-synthesized Au TNPs: (1) They have a large shape factor because of their atomically-flat two-dimensional structure.[20, 21, 46] Therefore, any minute change in the local refractive index substantially alters LSPR response. In this context, double-stranded nucleic acids that form between -ssDNAs/microRNAs display large polarizability because of high charge density, which should significantly modulate the local refractive index of TNPs and thus their LSPR sensitivity. (2) A high free carrier density is expected to reside at the sharp corners

and edges of TNPs that would lead to producing a large EM-field enhancement[47] at those places and consequently display large LSPR response during the receptor (-ssDNA) and analyte (microRNA) hybridization. (3) Recently, we demonstrated that a -ssDNA/microRNA duplex is capable of delocalizing electron wave functions of TNPs, which could result in a dramatic change in their free carrier density and thus influence LSPR properties and responses.[23]
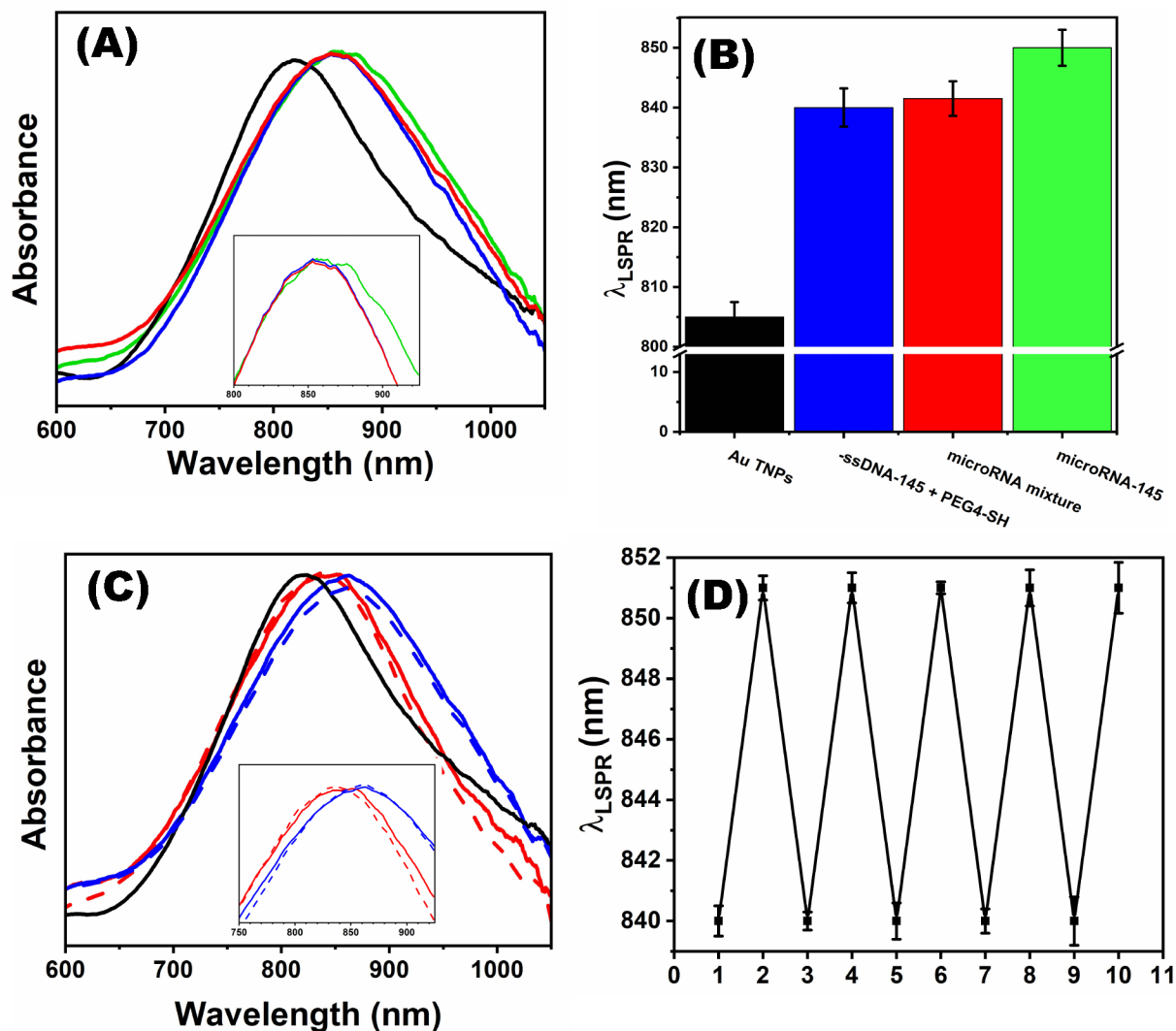
Figure 4. Specificity and Reversibility test. *(A)* *UV-visible extinction spectra of Au TNPs before (black curve, λ_{LSPR} =810 nm), after functionalized with –S-PEG$_4$: -S-(CH$_2$)$_3$-ssDNA-10b (blue curve, λ_{LSPR} = 845 nm), after incubation in a mixed solution of 10.0 nM concentration of microRNA-96, microRNA-145, microRNA-490-5p, and microRNA-143 (red curve, λ_{LSPR} = 846 nm), and after incubation in 10.0 nM microRNA-10b (green curve, λ_{LSPR} = 857 nm). All extinction spectra were collected in PBS buffer (pH = 7.2). Curve fitting through Origin software was applied to determine the exact λ_{LSPR} value. The inset shows an expanded region of the LSPR dipole peak of TNPs. (B) UV-visible extinction spectra of Au*

*TNPs before (black bar, λ_{LSPR} = 805 nm), after mixed –S-PEG$_4$: -S-(CH$_2$)$_3$-ssDNA-145 (blue bar, λ_{LSPR} = 840 nm) functionalization, after incubation in a mixed solution of 10.0 nM concentration of microRNA-10b, microRNA-96, microRNA-490-5p, and microRNA-143 (red bar, λ_{LSPR} = 841 nm), and after incubation in 10 nM microRNA-145 (green bar, λ_{LSPR} = 852 nm). All spectra were collected in PBS buffer (pH = 7.2). **(C)** UV-visible extinction spectra of Au TNPs (black curve, λ_{LSPR} = 805 nm), Au TNPs functionalized with –S-PEG$_4$: -S-(CH$_2$)$_3$-ssDNA-10b (red solid curve, λ_{LSPR} = 840 nm), after incubation in 10 nM microRNA-10b (blue solid curve, λ_{LSPR} = 851 nm), after incubation in RNase H enzyme solution (red dashed curve, λ_{LSPR} = 840 nm), and after 10 nM microRNA-10b again (blue dashed curve curve, λ_{LSPR} = 851 nm). The inset shows an expanded region of the LSPR dipole peak of TNPs. **(D)** Representation of the reversibility results, showing the biosensor is reversible up to 5 trials with trial 1 representing –ssDNA-10b incubation, trial 2, 4, 6, 8, and 10 representing microRNA-10b incubation, and trial 3,5,7, and 9 representing incubation in 15 unit of RNase H enzyme solution. All extinction spectra were normalized with Origin software.*

Specificity and Regenerative Characteristics of Biosensors. We examined the specificity of our plasmonic nanoantenna-based biosensors as this is critically important in clinical POC diagnostics. In practicality, biosensors with -ssDNA-10b- and PEG$_4$-S-functionalized Au TNPs should only display a $\Delta\lambda_{LSPR}$ value if an analyte solution contains microRNA-10b, which is an oncogenic microRNA for BC. As we have discussed above, there are several microRNAs that are up or down-regulated in BC, thus we incubated the above-mentioned constructed biosensors in plasma solutions containing microRNA-96, -145, -143, and -490-5p (10.0 nM/microRNA). As shown in **Figure 4A** (red curve), we measured $\Delta\lambda_{LSPR}$ values as high as 1.5 nm which is within the range of a false positive response for the biosensor (**Figure 3, Left**). Biosensors were then incubated in a 10.0 nM microRNA-10b solution and ~11 nm red shifts of λ_{LSPR} are observed **(Figure 4A,** green curve**)**. Since the LSPR shift only occurs in the presence of a complimentary microRNA sequence, we can safely state that our microRNA assay displays a high level of specificity without any false positive responses. In order to generalize the high specificity of our developed multiplexing biosensors, we also analyzed microRNA-145 utilizing the identical experimental approaches as described for microRNA-10b. **Figure 4B** illustrates experimentally determined λ_{LSPR} values at different incubation stages for the biosensors which was designed to specifically detect microRNA-145. The data are in agreement with high specificity towards detecting and quantifying only the target analyte.

Regeneration of biosensors is an important characteristic that would allow the same biosensor to be used for multiple patients and/or same patient sample for multiple trials to

mitigate false responses. This would provide an economically viable device, something critically important for potential applications in low income countries. Previously, we reported regenerative aspects of LSPR-based microRNA sensors.[20, 21] Here, we adopted similar experimental approaches to demonstrate the regenerative aspects of our multiplexing and high-throughput biosensors. As a proof-of-concept, we fabricated biosensors by functionalizing Au TNPs with -S-$(CH_2)_3$-ssDNA-10b: -S-PEG$_4$, which were then incubated in a 10.0 nM microRNA-10b solution. An ~11 nm λ_{LSPR} red shift (**Figure 4C**) is detected. The hybridized – ssDNA-10b/microRNA-10b functionalized biosensors were then incubated into 15 units RNase H enzyme solution for 2 hr and display an ~11 nm λ_{LSPR} blue shift. The position of λ_{LSPR} clearly suggests a full regeneration of our biosensors. The same biosensors were re-incubated in the microRNA-10b solution and nearly an identical λ_{LSPR} red shift is measured. Importantly, our plasmonic nanoantenna-based multiplexing microRNA biosensors can be regenerated for at least 5 cycles with a very negligible difference in sensing efficiency between the first and last trials (**Figure 4D**). We believe the unprecedentedly high stability of these plasmonic nanoantenna-based biosensors arises due to soft-soft covalent interactions between Au and S (from thiolated -ssDNA).[46] This stability is important for low cost clinical POC diagnosis as biosensors can be used several times without compromising their sensitivity.

Liquid Biopsy Utilizing Multiplexing and High-Throughput Biosensors. Liquid biopsies that involve analyzing circulating biomarkers (e.g., microRNAs) directly from patients' biofluids have shown tremendous promise in POC diagnosis. Liquid biopsies provide many advantages as they are noninvasive techniques that are less expensive and much simpler than tissue biopsies. To demonstrate the feasibility of multiplexing and high-throughput assay capabilities of our plasmonic nanoantenna-based biosensors in liquid biopsies, we employed our assay to analyze plasma samples of 20 BC patients (10 MTBC and 10 NMTBC) for each microRNA listed above. We selected BC patient samples for proof-of-concept liquid biopsies because the five-year survival rate of BC patients drastically drops, from 77% to 5%, when the disease is diagnosed at the metastasized state. Thus, early-stage diagnosis of BC is important in improving patient survival rates. However, the current FDA-approved urine cytology test is highly unreliable for early detection of BC. We analyzed 10 cancer-related (MTBC or NMTBC) patient plasma

samples, 5 NC plasma and 10 randomly selected wells for false positive and negative tests all

within a single 96 well-plate biosensor from a single instrument run.
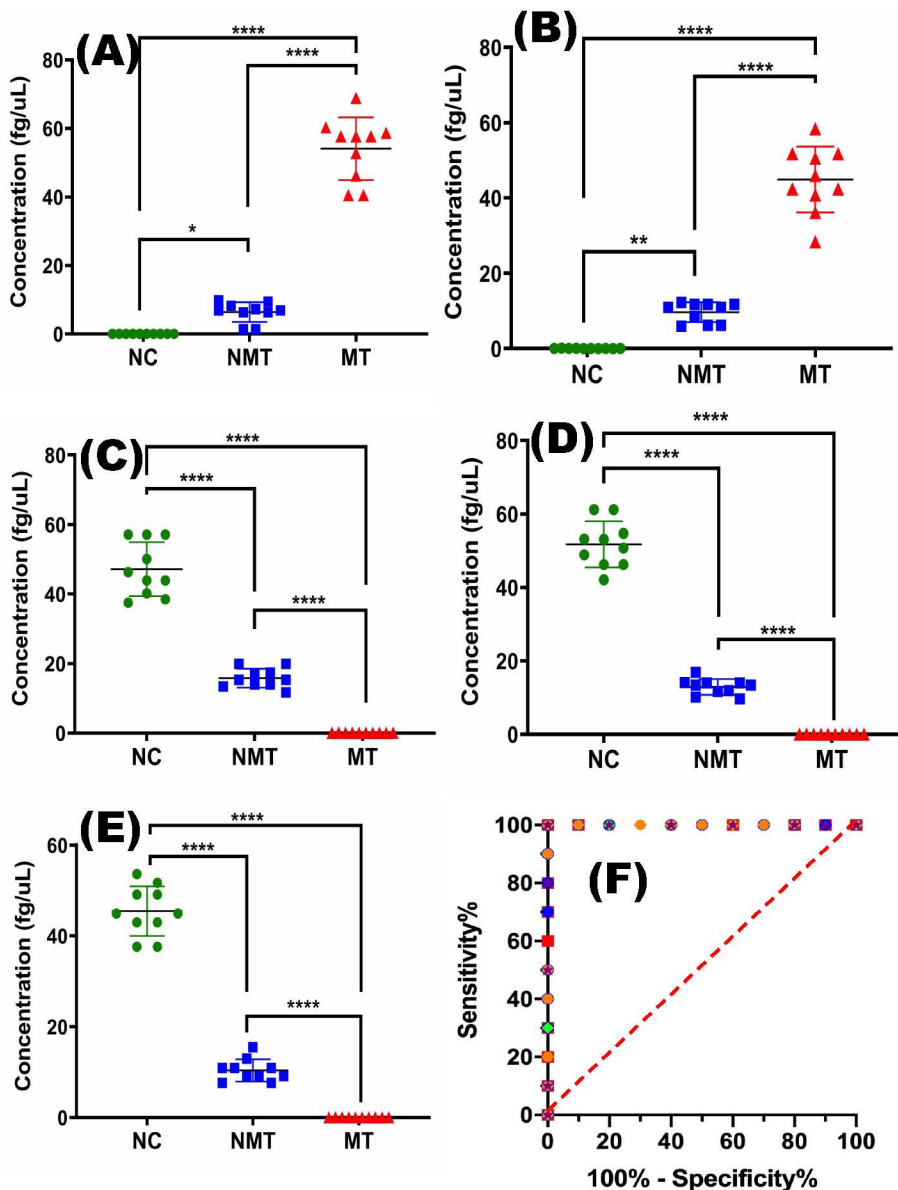
Figure 5. **Plasmonic nanoantenna-based multiplexing and high-throughput liquid biopsies.**
*ANOVA results of normal control verses non-metastatic verses metastatic patient samples for **(A)**
microRNA-10b, **(B)** microRNA-96, **(C)** microRNA-145, **(D)** microRNA-143, and **(E)** microRNA-490-5p.
(F) Receiver operating characteristic curve of normal control verses metastatic patient samples. [Red
squares = microRNA-10b, blue circles = microRNA-96, green diamonds = microRNA-145, orange
hexagons = microRNA-143, and purple stars = microRNA-490-5p.] p (ns) = 0.1234, *P < 0.0332, **P
< 0.0021, ***P< 0.0002, ****P<0.0001 by one-way ANOVA.*

As shown in **Figure 5A-E,** results show that both oncogenic and tumor suppressor microRNAs can be used as biomarkers to distinguish the cancer stages. However, tumor suppressor microRNAs (microRNA-145, -143, -490-5p) are found to be more selective biomarkers (**Figure 5C-E**) with a p-value < 0.0001 for MTBC patients vs. NC, NMTBC patients vs. NC, and MTBC vs NMTBC patients in comparison to oncogenic microRNAs (microRNA-10b and -96). Therefore, based on the LSPR-based biosensing, it is safe to state that tumor suppressor microRNAs represent a more accurate biomarker for early-stage diagnostic of BC. As illustrated in **Figure 5F and Figure S2D**, ROC analysis reveals that plasmonic nanoantenna-based biosensing is highly accurate and discriminates between the control group (NC) versus the disease group (MT or NMT patients) with an AUC of 1.0. We envision that the high-throughput capability of the current assay can be expanded to 384 well-plates for analysis of a larger number of patient samples simultaneously.

CONCLUSION

In summary, we have developed multiplexing and high-throughput biosensors utilizing the unique LSPR properties of plasmonic nanoantennas, which allow the ultrasensitive and quantitative measure of microRNAs through liquid biopsies. In the bottom up fabrication approach presented, we used chemically-synthesized plasmonic nanoantennas of different shapes (Au TNPs, NRs and SNPs). Bulk refractive index sensitivity studies showed that among these nanoantennas shapes, Au TNPs were most sensitive, with a sensitivity as high as 318 nm/RIU. Our newly developed and highly specific multiplexing assay is capable of quantifying five different types of microRNAs with an LOD of ~100 aM. Furthermore, our plasmonic nanoantenna-based biosensors are both stable and regenerative, up to 5 cycles without compromising sensitivity. As a proof-of-concept, in utilizing the multiplexing and high-throughput capabilities of these biosensors, liquid biopsies were conducted directly from the unmodified plasma of 20 patients with BC. Results showed an unprecedentedly high specificity (p value of <0.0001 and an AUC equal to 1.0) and demonstrated that our assay is not only capable of diagnosing BC at an early stage, but also distinguishing BC in different stages. Taken together, we believe that the high specificity and stability of microRNA biosensors, along with their multiplexing and high-throughput capabilities, will significantly advance the biosensing

field by providing a POC-applicable approach to perform early stage diagnosis and prognosis of diseases using microRNA or other biomarkers (e.g., proteins and mRNA). Importantly, because of these unique advantages of plasmonic nanoantenna-based biosensors, their potential applications are far-reaching, for not only cancer diagnostic but also detecting infectious diseases including severe acute respiratory syndrome coronavirus 2 (SARS-CoV-2, also called COVID-19) in a POC set-up.

ASSOCIATED CONTENT

Supporting Information Available. Additional experimental procedures, UV-visible extinction spectra, tables, calibration plots, LSPR shift bar graphs, and ROC plot. These materials are available free of charge. (PDF)

AUTHOR INFORMATION

Corresponding Author

* Email: rsardar@iupui.edu

AUTHOR CONTRIBUTIONS
A.N.M. and R.S. designed experiments, A.N.M. and T.L. conducted all sensing measurements and analyzed data. H.G.D. provided guidance in Au NR synthesis. H.K. collected all BC related patients' plasma samples and verified disease states. F.D. helped in optical measurements. A.N.M. and R.S edited and revised the manuscript for appropriate presentation of the findings. All authors discussed the results and contributed to the final manuscript.

References

1.   Mayer, K. M.; Hafner, J. H., *Chem. Rev.* **2011,** *111* (6), 3828-3857.

2.   Stewart, M. E.; Anderton, C. R.; Thompson, L. B.; Maria, J.; Gray, S. K.; Rogers, J. A.; Nuzzo, R. G., *Chem. Rev.* **2008,** *108* (2), 494-521.

3.   Jain, P. K.; Huang, X.; El-Sayed, I. H.; El-Sayed, M. A., *Accounts of Chemical Research* **2008,** *41* (12), 1578-1586.

4.   Halas, N. J.; Lal, S.; Chang, W.-S.; Link, S.; Nordlander, P., *Chem. Rev.* **2011,** *111* (6), 3913-3961.

5.   Joshi, G. K.; Smith, K. A.; Johnson, M. A.; Sardar, R., *Journal of Physical Chemistry C* **2013,** *117* (49), 26228-26237.

6.   Jin, S.-Q.; Ye, B.-C.; Huo, H.; Zeng, A.-J.; Xie, C.-K.; Ren, B.-Q.; Huang, H.-J., *Anal. Chem.* **2010,** *82* (23), 9925-9931.

7.   Vreeland, W. N.; Meagher, R. J.; Barron, A. E., *Analytical Chemistry* **2002,** *74* (17), 4328-4333.

8.   Gonzalez, R. M.; Seurynck-Servoss, S. L.; Crowley, S. A.; Brown, M.; Omenn, G. S.; Hayes, D. F.; Zangar, R. C., *Journal of Proteome Research* **2008,** *7* (6), 2406-2414.

9.   Han, K.-C.; Ahn, D.-R.; Yang, E.-G., *Bioconjugate Chemistry* **2010,** *21* (12), 2190-2196.

10.   Hu, R.; Liu, T.; Zhang, X.-B.; Yang, Y.; Chen, T.; Wu, C.; Liu, Y.; Zhu, G.; Huan, S.; Fu, T.; Tan, W., *Analytical Chemistry* **2015,** *87* (15), 7746-7753.

11.   Dong, J.; Salem, D. P.; Sun, J. H.; Strano, M. S., *ACS Nano* **2018,** *12* (4), 3769-3779.

12.   Falconnet, D.; She, J.; Tornay, R.; Leimgruber, E.; Bernasconi, D.; Lagopoulos, L.; Renaud, P.; Demierre, N.; van den Bogaard, P., *Anal. Chem.* **2015,** *87* (3), 1582-1589.

13.   Nagarajan, M. B.; Tentori, A. M.; Zhang, W. C.; Slack, F. J.; Doyle, P. S., *Analytical Chemistry* **2018,** *90* (17), 10279-10285.

14.   Chen, S.; Dou, Y.; Zhao, Z.; Li, F.; Su, J.; Fan, C.; Song, S., *Anal. Chem.* **2016,** *88* (7), 3476-3480.

15.   Pheeney, C. G.; Arnold, A. R.; Grodick, M. A.; Barton, J. K., *Journal of the American Chemical Society* **2013,** *135* (32), 11869-11878.

16.   Zeng, D.; Wang, Z.; Meng, Z.; Wang, P.; San, L.; Wang, W.; Aldalbahi, A.; Li, L.; Shen, J.; Mi, X., *ACS Applied Materials & Interfaces* **2017,** *9* (28), 24118-24125.

17.   Beeram, S. R.; Zamborini, F. P., *Journal of the American Chemical Society* **2009,** *131* (33), 11689-11691.

18.   Mejia-Salazar, J. R.; Oliveira, O. N., *Chem. Rev.* **2018,** *118* (20), 10617-10625.

19.   Saha, K.; Agasti, S. S.; Kim, C.; Li, X.; Rotello, V. M., *Chem. Rev.* **2012,** *112* (5), 2739-2779.

20.   Joshi, G. K.; Deitz-McElyea, S.; Johnson, M.; Mali, S.; Korc, M.; Sardar, R., *Nano Letters* **2014,** *14* (12), 6955-6963.

21.   Joshi, G. K.; Deitz-McElyea, S.; Liyanage, T.; Lawrence, K.; Mali, S.; Sardar, R.; Korc, M., *ACS Nano* **2015,** *9* (11), 11075-11089.

22.   Joshi, G. K.; McClory, P. J.; Muhoberac, B. B.; Kumbhar, A.; Smith, K. A.; Sardar, R., *Journal of Physical Chemistry C* **2012,** *116* (39), 20990-21000.

23.   Liyanage, T.; Masterson, A. N.; Oyem, H. H.; Kaimakliotis, H.; Nguyen, H.; Sardar, R., *Anal. Chem.* **2019,** *91* (3), 1894-1903.

24.   He, J.; Boegli, M.; Bruzas, I.; Lum, W.; Sagle, L., *Anal. Chem.* **2015,** *87* (22), 11407-11414.

25.   Rosman, C.; Prasad, J.; Neiser, A.; Henkel, A.; Edgar, J.; Soennichsen, C., *Nano Letters* **2013,** *13* (7), 3243-3247.

26.   Winter, J.; Jung, S.; Keller, S.; Gregory, R. I.; Diederichs, S., *Nature Cell Biology* **2009,** *11* (3), 228-234.

27.   He, L.; Thomson, J. M.; Hemann, M. T.; Hernando-Monge, E.; Mu, D.; Goodson, S.; Powers, S.; Cordon-Cardo, C.; Lowe, S. W.; Hannon, G. J.; Hammond, S. M., *Nature* **2005,** *435* (7043), 828-833.

28.   Esquela-Kerscher, A.; Slack, F. J., *Nature Reviews Cancer* **2006,** *6* (4), 259-269.

29.   Wang, J.; Chen, J.; Sen, S., *Journal of Cellular Physiology* **2016,** *231* (1), 25-30.

30.   Xiao, H.; Li, H.; Yu, G.; Xiao, W.; Hu, J.; Tang, K.; Zeng, J.; He, W.; Zeng, G.; Ye, Z.; Xu, H., *Oncology Reports* **2014,** *31* (4), 1832-1838.

31.   Wu, Z.; Liu, K.; Wang, Y.; Xu, Z.; Meng, J.; Gu, S., *Cancer Cell International* **2015,** *15*, 107/1-107/9.

32.   Lin, T.; Dong, W.; Huang, J.; Pan, Q.; Fan, X.; Zhang, C.; Huang, L., *J. Urol.* **2009,** *181* (3), 1372-1380.

33.   Li, S.; Xu, X.; Xu, X.; Hu, Z.; Wu, J.; Zhu, Y.; Chen, H.; Mao, Y.; Lin, Y.; Luo, J.; Zheng, X.; Xie, L., *Biochemical and Biophysical Research Communications* **2013,** *441* (4), 976-981.

34.   Lan, G.; Yang, L.; Xie, X.; Peng, L.; Wang, Y., *Archives of Medical Science* **2015,** *11* (3), 561-569.

35.   Chiyomaru, T.; Enokida, H.; Tatarano, S.; Kawahara, K.; Uchida, Y.; Nishiyama, K.; Fujimura, L.; Kikkawa, N.; Seki, N.; Nakagawa, M., *British Journal of Cancer* **2010,** *102* (5), 883-891.

36.   Prusty, G.; Lee, J. T.; Seifert, S.; Muhoberac, B. B.; Sardar, R., *Journal of the American Chemical Society* **2020,** *142* (13), 5938-5942.

37.   Jain, P. K.; El-Sayed, M. A., *Journal of Physical Chemistry C* **2007,** *111* (47), 17451-17454.

38.   Kelly, K. L.; Coronado, E.; Zhao, L. L.; Schatz, G. C., *Journal of Physical Chemistry B* **2003,** *107* (3), 668-677.

39.   Chen, H.; Kou, X.; Yang, Z.; Ni, W.; Wang, J., *Langmuir* **2008,** *24* (10), 5233-5237.

40.   Nath, N.; Chilkoti, A., *Analytical Chemistry* **2004,** *76* (18), 5370-5378.

41.   Basiruddin, S.; Saha, A.; Pradhan, N.; Jana, N. R., *Langmuir* **2010,** *26* (10), 7475-7481.

42.   Castellana, E. T.; Gamez, R. C.; Russell, D. H., *Journal of the American Chemical Society* **2011,** *133* (12), 4182-4185.

43.   Gole, A.; Murphy, C. J., *Chemistry of Materials* **2005,** *17* (6), 1325-1330.

44.   Liao, H.; Hafner, J. H., *Chemistry of Materials* **2005,** *17* (18), 4636-4641.

45.   Mbalaha, Z. S.; Edwards, P. R.; Birch, D. J. S.; Chen, Y., *ACS Omega* **2019,** *4* (9), 13740-13746.

46.   Liyanage, T.; Nagaraju, M.; Johnson, M.; Muhoberac, B. B.; Sardar, R., *Nano Letters* **2020,** *20* (1), 192-200.

1
2
3
4
5
6
7
8
9
10
11
12
13
14
15
16
17
18
19
20
21
22
23
24
25
26
27
28
29
30
31
32
33
34
35
36
37
38
39
40
41
42
43
44
45
46
47
48
49
50
51
52
53
54
55
56
57
58
59
60

47.   Liyanage, T.; Rael, A.; Shaffer, S.; Zaidi, S.; Goodpaster, J. V.; Sardar, R., *Analyst* **2018,** *143* (9), 2012-2022.

TOC Graphic